



Common germline variants of the human *APOE* gene modulate melanoma progression and survival

Benjamin N. Ostendorf¹ , Jana Bilanovic¹, Nneoma Adaku¹, Kimia N. Tafreshian¹, Bernardo Tavora¹, Roger D. Vaughan² and Sohail F. Tavazoie¹  

Common germline variants of the *APOE* gene are major risk modifiers of neurodegenerative and atherosclerotic diseases^{1–3}, but their effect on cancer outcome is poorly defined. Here we report that, in a reversal of their effect on Alzheimer's disease, the *APOE4* and *APOE2* variants confer favorable and poor outcomes in melanoma, respectively. Mice expressing the human *APOE4* allele exhibited reduced melanoma progression and metastasis relative to *APOE2* mice. *APOE4* mice exhibited enhanced anti-tumor immune activation relative to *APOE2* mice, and T cell depletion experiments showed that the effect of *APOE* genotype on melanoma progression was mediated by altered anti-tumor immunity. Consistently, patients with melanoma carrying the *APOE4* variant experienced improved survival in comparison to carriers of *APOE2*. Notably, *APOE4* mice also showed improved outcomes under PD1 immune checkpoint blockade relative to *APOE2* mice, and patients carrying *APOE4* experienced improved anti-PD1 immunotherapy survival after progression on frontline regimens. Finally, enhancing *APOE* expression via pharmacologic activation of liver X receptors, previously shown to boost anti-tumor immunity⁴, exhibited therapeutic efficacy in *APOE4* mice but not in *APOE2* mice. These findings demonstrate that pre-existing hereditary genetics can impact progression and survival outcomes of a future malignancy and warrant prospective investigation of *APOE* genotype as a biomarker for melanoma outcome and therapeutic response.

The secreted glycoprotein APOE exerts pleiotropic effects on organismal metabolism and immunity^{3,5}. In humans, there are three highly prevalent genetic variants of *APOE*, termed *APOE2*, *APOE3* and *APOE4*. The products of these gene variants differ by only one or two amino acids but exhibit differential binding to, and activation of, APOE receptors (Fig. 1a)^{6–9}. Notably, the *APOE4* variant is the largest monogenetic risk factor for Alzheimer's disease, whereas *APOE2* is protective^{1,2}. In addition, *APOE* variants modulate other inflammation-associated pathologies, including atherosclerosis³. The potential association between *APOE* genotype and cancer outcome has remained inconclusive^{10,11}. We previously reported that tumoral and stroma-derived APOE suppress melanoma progression^{4,12,13}. In contrast to tumoral APOE, for which expression becomes repressed during melanoma progression, stroma-derived APOE expression is dictated by the genetics of the host¹². We thus reasoned that distinct *APOE* germline variants might differentially regulate melanoma progression and tested this hypothesis through experimental and clinical association approaches.

To assess whether host *APOE* variants affect melanoma outcome, we used mice in which the endogenous murine *ApoE* locus had been

replaced with human *APOE* variants^{14–16}. Remarkably, progression of syngeneic YUMM1.7 mouse melanoma tumors was significantly slower in *APOE4* mice than in *APOE2* mice (Fig. 1b). We validated these findings in the independent YUMM3.3 model and in the YUMMER1.7 melanoma model, a more immunogenic derivative of the YUMM1.7 model¹⁷ (Fig. 1c,d). To assess the effect of *APOE* genotype on melanoma metastasis, we used B16F10 melanoma cells, which reproducibly metastasize in tail vein colonization assays. Consistent with our observations in primary tumor progression, *APOE4* mice showed reduced metastatic progression compared to *APOE2* mice (Extended Data Fig. 1a,b). Thus, stromal *APOE* genotype causally affected progression in murine melanoma models.

APOE modulates immune responses in several different contexts^{18–21}. In cancer, APOE enhances anti-tumor immunity by modulating myeloid immune cell populations⁴. We therefore sought to determine whether APOE variants differentially affect the immune response in cancer. Flow cytometry revealed enhanced recruitment of CD45⁺ leukocytes into melanoma tumors hosted by *APOE4* mice compared to *APOE2* mice (Fig. 2a and Extended Data Fig. 2a–d). The proportions of immunosuppressive Ly6G⁺ granulocytic myeloid-derived suppressor cells (G-MDSCs) and tumor-associated macrophages were reduced in *APOE4* mice relative to *APOE2* mice (Fig. 2b). Concomitantly, we observed increased proportions of anti-tumor effector cells in *APOE4* mice, such as natural killer (NK) and CD8⁺ T cells (Fig. 2c). We validated enhanced CD8⁺ T cell recruitment into tumors hosted by *APOE4* versus *APOE2* mice by histology (Extended Data Fig. 2e). Intracellular flow cytometry revealed enhanced activation of NK, CD4⁺ and CD8⁺ T cells in *APOE4* mice relative to *APOE2* mice, as illustrated by increased granzyme B and interferon- γ expression (Fig. 2d–f). To more comprehensively characterize the immune microenvironment, we performed single-cell RNA-sequencing (scRNA-seq) of CD45⁺ leukocytes sorted from tumors in *APOE* variant mice (Fig. 2g and Extended Data Fig. 3a). Consistent with the flow cytometry results, *APOE4* hosts exhibited expansion and activation of NK and CD8⁺ T effector cells, as well as profound shifts in the myeloid compartment (Fig. 2h and Extended Data Fig. 3b–d). Analysis of differentially expressed genes in individual clusters between *APOE4* and *APOE2* mice revealed enrichment of pathways implicated in anti-tumor immune activity, such as interferon signaling. This was accompanied by depletion of pathways implicated in pro-tumor phenotypes, such as angiogenesis (Fig. 2i). These data suggest that *APOE* genotype modulated both the abundance and the functional state of the tumor immune microenvironment, with the *APOE4* variant eliciting an enhanced anti-tumor immune profile relative to the *APOE2* variant.

¹Laboratory of Systems Cancer Biology, The Rockefeller University, New York, NY, USA. ²Department of Biostatistics, The Rockefeller University, New York, NY, USA. ✉e-mail: stavazoie@rockefeller.edu

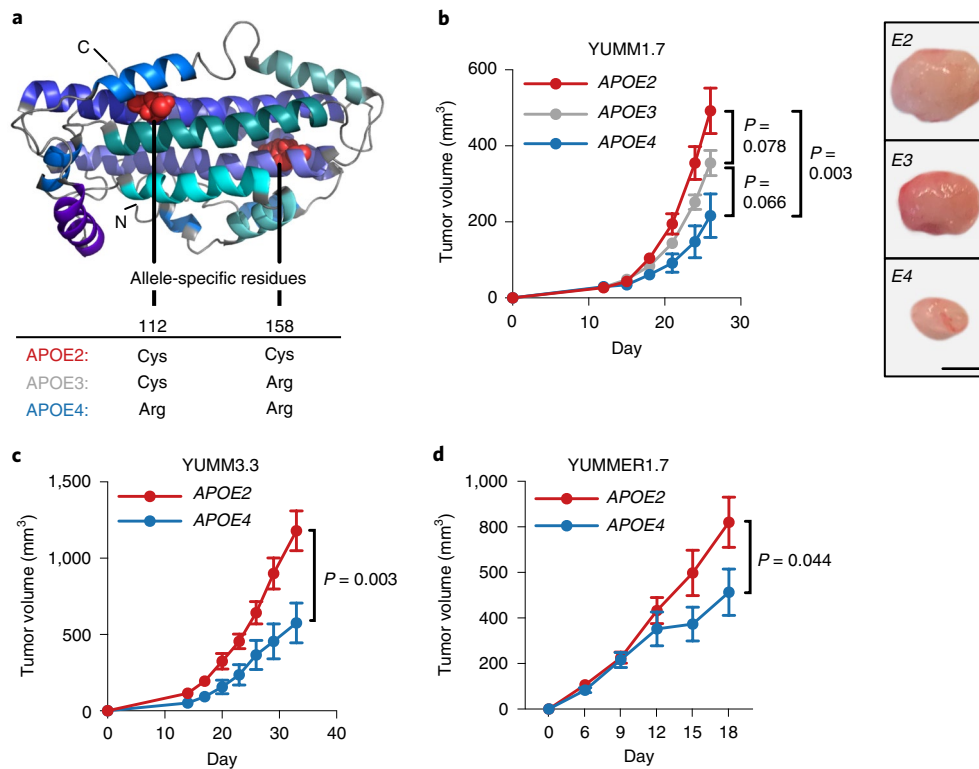


Fig. 1 | Human APOE variants modulate progression of murine melanoma. a, Structural representation of APOE3 (based on the structure by Chen et al.⁶). **b**, Growth of murine YUMM1.7 tumors in APOE knock-in mice ($n=11$ mice per group, representative of two independent experiments). Representative tumors correspond to day 26 (scale bar, 3 mm). **c**, Growth of murine YUMM3.3 melanomas in human APOE knock-in mice ($n=13$ mice per group, representative of two independent experiments). **d**, Growth of murine YUMMER1.7 melanomas in APOE knock-in mice ($n=13$ and 11 mice for APOE2 and APOE4, respectively; representative of two independent experiments). Graphs represent mean values \pm s.e.m. All P values are based on two-tailed t -tests.

We next sought to investigate whether immune modulation causally mediated the differential effect of APOE genotype on melanoma progression. Remarkably, T cell depletion completely abrogated growth differences of YUMM1.7 tumors in APOE4 versus APOE2 mice (Fig. 2j and Extended Data Fig. 4). To assess whether the hematopoietic cell compartment could mediate APOE genotype-dependent effects on melanoma progression, we transplanted hematopoietic stem cells from APOE4 and APOE2 mice into lethally irradiated wild-type mice harboring the murine *ApoE* gene. YUMM1.7 tumor progression was slower in mice transplanted with APOE4 versus APOE2 bone marrow (Fig. 2k,l). Thus, APOE genotype affected melanoma progression by modulating the anti-tumor immune response, and APOE genotype within the hematopoietic compartment was sufficient to drive differential melanoma progression.

In addition to its immunomodulatory effects, APOE exerts pleiotropic anti-tumor effects in part by suppressing melanoma cell invasion and endothelial recruitment¹². We therefore assessed whether APOE variants could also differentially affect these tumoral phenotypes. Indeed, recombinant APOE4 protein was more efficient than APOE2 in suppressing invasion of melanoma cells (Extended Data Fig. 5a). APOE4 was also more potent than APOE2 in suppressing endothelial recruitment by melanoma cells (Extended Data Fig. 5b). Consistent with this in vitro finding, blood vessel density in vivo in YUMM1.7 tumors was significantly reduced in APOE4 versus APOE2 mice (Extended Data Fig. 5c). Thus, APOE variants differentially affected multiple key phenotypes associated with enhanced tumor progression and metastasis.

To determine if APOE genotype associates with outcomes in human melanoma, we assessed germline APOE variant status in patients from The Cancer Genome Atlas (TCGA) who were

originally diagnosed with primary melanomas at risk for relapse (stage II and III) (Fig. 3a)²². Neither APOE2 nor APOE4 carriers were enriched in the TCGA skin cutaneous melanoma (SKCM) study in comparison to a control group with similar age and ethnic composition²³, indicating that neither genotype associated with increased melanoma incidence (Extended Data Fig. 6a,b). Strikingly, however, APOE carrier status was significantly associated with survival (median survival of 2.4, 5.2, and 10.1 years in APOE2 carriers, APOE3 homozygotes and APOE4 carriers, respectively; $P=0.0038$, log-rank test; Fig. 3b). Cox proportional hazard regression analysis revealed an increased hazard ratio (HR) in this data set for APOE2 carriers versus APOE3 homozygotes (HR = 2.08, $P=0.01$) and versus APOE4 carriers (HR = 3.69, $P<0.001$) (Fig. 3c). There were no significant differences between APOE carrier groups in potentially confounding clinical characteristics at the time of diagnosis, and APOE genotype remained significantly associated with survival in a multivariable analysis (Extended Data Fig. 7). The distribution of APOE carrier status was not significantly different between normal tissue and tumor samples, and the same carrier status was identified in sample pairs of 95.6% of individuals with available results (94.2% of all samples) (Extended Data Fig. 8), suggesting our genotyping approach to be robust and loss-of-heterozygosity events in the tumor to be rare. Our observation of improved melanoma survival outcomes of APOE4 carriers relative to APOE2 carriers was especially surprising because APOE4 status associates with reduced longevity and would thus be expected to counter potential enhanced cancer survival effects²⁴. We reasoned that our ability to observe this effect of APOE genotype on survival was likely due to the fact that survival in the TCGA melanoma study was primarily determined by the high rates of melanoma-associated death in this group of high-risk patients^{22,25}. To validate these findings in an independent

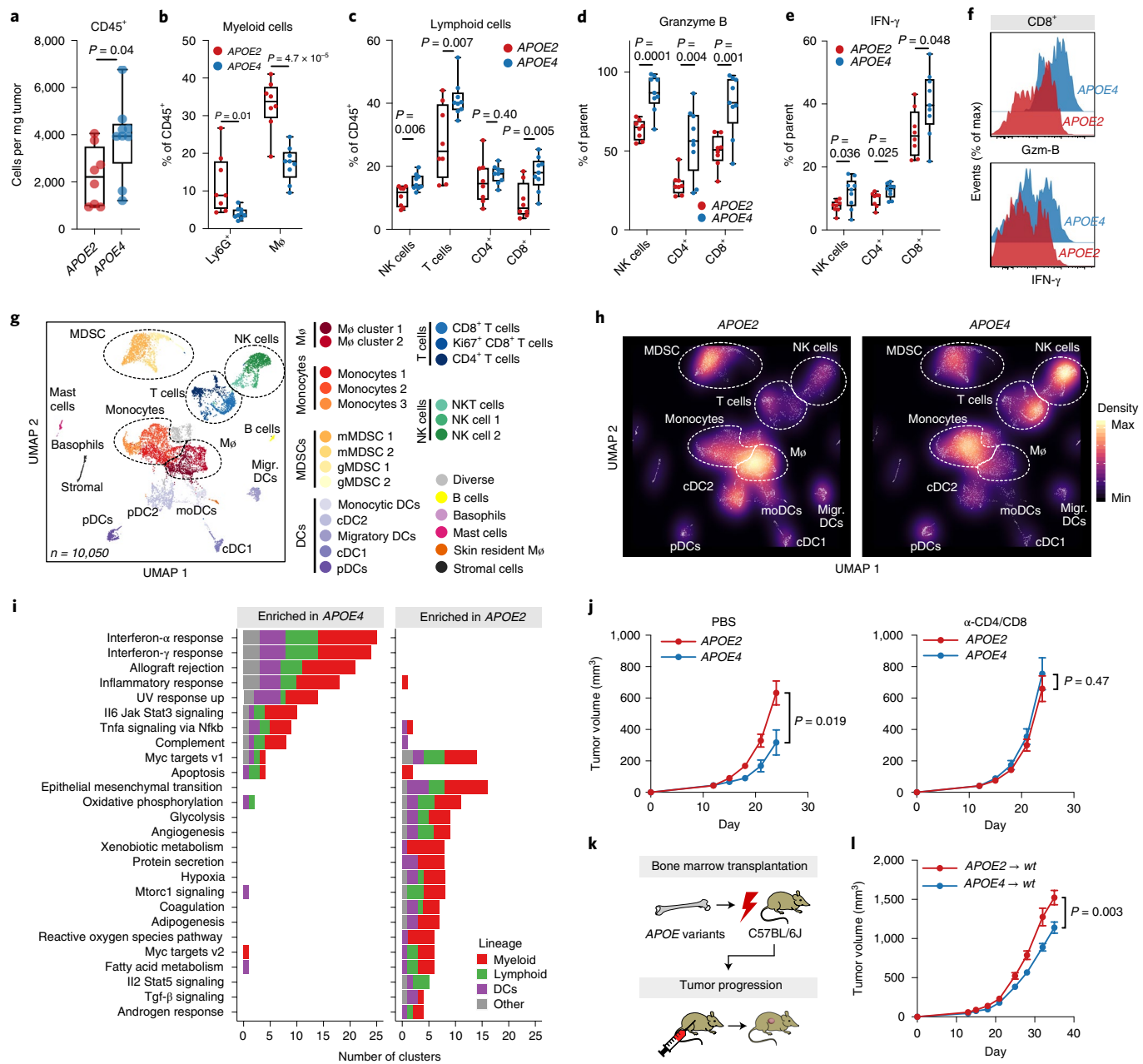


Fig. 2 | Human *APOE* variants modulate the tumor immune microenvironment. **a**, Abundance of CD45⁺ leukocytes in YUMM1.7 tumors in *APOE2* and *APOE4* knock-in mice (two-tailed *t*-test). **b,c**, Proportion of tumor-infiltrating myeloid (**b**) and lymphoid (**c**) immune subsets in YUMM1.7 melanoma-bearing *APOE2* and *APOE4* mice (two-tailed *t*-tests). **d,e**, Expression of granzyme B (Gzm-B) (**d**) and interferon- γ (IFN- γ) (**e**) in immune effector cells infiltrating YUMM1.7 melanomas in *APOE2* versus *APOE4* mice (one-tailed *t*-tests). **f**, Representative flow cytometry plots from **d** and **e** illustrating the expression of activation markers in YUMM1.7-infiltrating CD8⁺ T cells in *APOE2* and *APOE4* mice. **g**, UMAP plot of 10,050 CD45⁺ RNA-sequenced tumor-infiltrating immune cells from *APOE2* and *APOE4* hosts. **h**, Density plot of **g** stratified by *APOE* genotype. **i**, Number of immune cell clusters as identified by scRNA-seq with pathway enrichment in genes differentially expressed between *APOE4* and *APOE2* (pathways listed with significance in >3 clusters; significance based on two-sided permutation testing and adjusted for number of tested pathways by false discovery rate). **j**, Effect of T cell depletion on YUMM1.7 tumor growth in human *APOE* knock-in mice ($n = 24, 11, 11$ and 10 mice for *APOE2*/PBS, *APOE4*/PBS, *APOE2*/depletion and *APOE4*/depletion groups, respectively; two-tailed *t*-tests; representative of two independent experiments). **k**, Experimental approach to determine the effect of hematopoietic cell-derived *APOE* variants on melanoma progression. **l**, Growth of YUMM1.7 tumors in C57BL/6J wild-type mice transplanted with bone marrow from human *APOE* knock-in mice ($n = 15$ per group, two-tailed *t*-test). Box plots in **a–f** show median, and whiskers represent minimum and maximum. For **a–f**, $n = 8$ and $n = 9$ mice for *APOE2* and *APOE4* groups, respectively, and data are representative of two independent experiments. Graphs in **j** and **l** represent mean values \pm s.e.m. For **g–i**, $n = 6$ biologically averaged mice per group.

study, we imputed *APOE* genotype in a melanoma genome-wide association study (GWAS)²⁶ (Extended Data Fig. 9a,b). Consistent with our findings in the TCGA-SKCM study, *APOE2* genotype was associated with the shortest survival in patients at high risk

of melanoma-associated death (Clark level 5). In contrast, *APOE2* carriers trended toward better survival in patients with low risk of melanoma-associated death (Extended Data Fig. 9c–g), consistent with the known association of *APOE2* with enhanced lifespan in

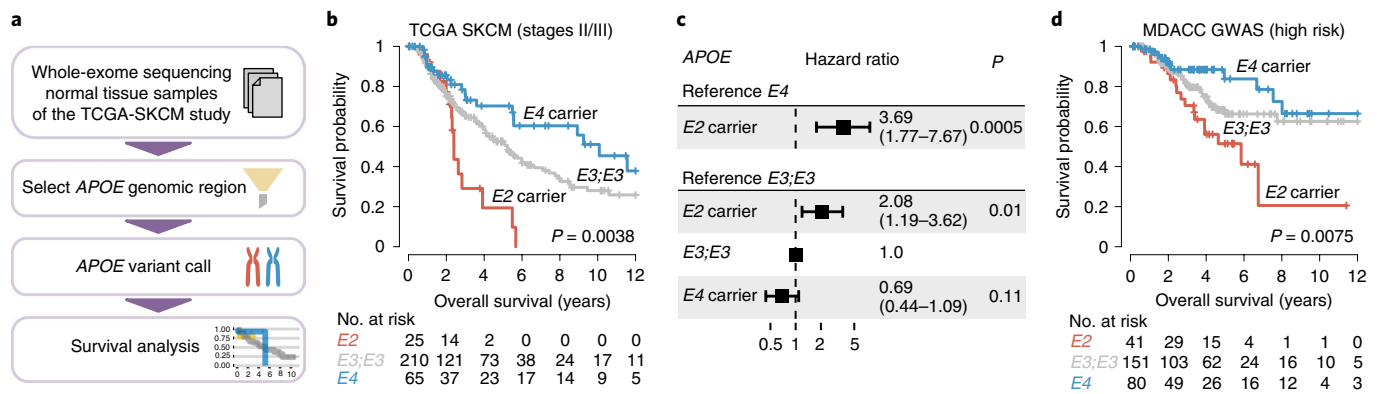


Fig. 3 | *APOE* germline variants predict survival in human melanoma. a, Computational pipeline to analyze the effect of *APOE* genotype on melanoma outcome in the TCGA-SKCM study. **b, c**, Survival (**b**) and HRs (**c**) of patients with stage II and III melanoma in the TCGA-SKCM study stratified by *APOE* carrier status (P values according to two-sided log-rank test (**b**) and two-sided Cox proportional hazard model (**c**); numbers in parentheses indicate 95% confidence intervals). **d**, Survival of patients with high-risk melanoma in the MDACC GWAS study as defined by advanced local melanoma and older age (P value according to two-sided log-rank test).

the general population²⁴. Of note, overall survival of patients in the MD Anderson Cancer Center (MDACC) study was significantly better than survival in the TCGA study, likely attributable to significant differences in factors predisposing for better outcomes, such as younger age and lower Clark level (Extended Data Fig. 9h–k). Indeed, restricting the analysis to the subset of patients at the highest risk for relapse and melanoma-associated death, as defined by age and high Clark level, revealed a pronounced association of *APOE* genotype with survival in this data set (Fig. 3d), mirroring the findings in the TCGA study. Thus, germline genetic variants of *APOE* differentially associated with survival in patients with advanced melanoma who were at increased risk for melanoma-associated death and metastasis.

Immunotherapy has transformed melanoma treatment^{27–29}, prompting us to assess whether *APOE* genotype could also affect melanoma progression in the context of immunotherapy. To this end, we analyzed the effect of *APOE* genotype on progression of the immunogenic YUMMER1.7 melanoma model, which is susceptible to anti-PD1 checkpoint therapy¹⁷. *APOE4* mice survived significantly longer than *APOE2* mice upon anti-PD1 treatment, suggesting that *APOE* genotype modulates melanoma outcome also in the context of immunotherapy (Fig. 4a,b). To assess whether this effect could also be observed in humans, we analyzed patients with melanoma who received anti-PD1 checkpoint inhibition therapy after progressing on anti-CTLA4 checkpoint blockade³⁰. Indeed, *APOE* genotype was significantly associated with survival in this study. Consistent with our observations on survival of mostly non-immunotherapy-treated patients of the TCGA and MDACC studies described above, *APOE4* and *APOE2* carriers exhibited the longest and shortest survival outcomes, respectively, upon anti-PD1 therapy (Fig. 4c). We validated these findings in an independent study of patients receiving anti-PD1 therapy upon progressing on CTLA4 blockade³¹. *APOE4* and *APOE2* carriers in this study also exhibited the longest and shortest survival outcomes, respectively (Fig. 4d). Thus, in both of these studies, *APOE* genotype associated with survival in patients who had progressed on prior immunotherapy. We observed no significant effect of *APOE* genotype on survival in patients in the study of Riaz et al. who received PD1 blockade with no prior checkpoint immunotherapy (Extended Data Fig. 10). This could either be due to the small sample size or suggest a potential contextual basis for *APOE*-dependent modulation of immunotherapy outcome.

Finally, we reasoned that pharmacologic activation of *APOE* might augment the differential effect of *APOE* variants on melanoma

progression. Liver X receptors (LXRs) are nuclear hormone receptors that transcriptionally activate several genes implicated in cholesterol and lipid metabolism, including *APOE*^{32,33}. LXR agonism has been shown to enhance anti-tumor immunity—an effect primarily mediated by *APOE*^{4,13}. Indeed, the efficacy of LXR agonism was completely abrogated in *APOE2* mice, whereas *APOE4* mice benefited from robust anti-tumor effects of treatment, augmenting the differences in tumor progression between *APOE2* and *APOE4* mice (Fig. 4e,f). Thus, distinct *APOE* genotypes elicited differential responsiveness to LXR agonistic therapy and might serve as potential genetic biomarkers for current clinical efforts investigating the use of LXR agonism in cancer therapy⁴.

APOE variants modulate multiple inflammation-associated pathologies. Our work provides causal evidence that, in a reversal of their role in neurodegenerative diseases, the highly prevalent *APOE4* and *APOE2* variants confer favorable and poor progression outcomes in melanoma, respectively, by affecting anti-tumor immunity. Previous reports revealed differential activation of *APOE* receptors by *APOE* variants, potentially explaining the differential biological effect of these variants^{7–9}. *APOE2* has been shown to exhibit reduced binding to *APOE* receptors^{7,8}. In contrast, *APOE4* has been observed to exhibit enhanced receptor binding and/or signaling^{9,34}. Our findings in this report are consistent with these past biochemical observations of enhanced (*APOE4*) and reduced (*APOE2*) *APOE* function in cancer, given the previously described roles of *APOE* in suppressing innate immune suppression, invasiveness and endothelial recruitment^{4,12}. Of note, despite the multitude of potential mechanisms that have been invoked to explain the effect of *APOE* variants on Alzheimer's disease risk, a unifying explanation remains elusive, likely stemming from *APOE*'s pleiotropic organismal effects. In analogy, future studies will need to explore whether additional mechanisms account for the effect of *APOE* genotype on melanoma progression.

Our findings have several potential clinical implications. Most importantly, they suggest that common germline variants might serve as biomarkers to identify patients with melanoma who are at high risk for metastatic relapse and melanoma-associated death for treatment with adjuvant systemic therapy. Notably, these clinical association findings will need to be assessed in prospective studies. It will be important to also assess the effect of *APOE* genotype on the outcome of additional cancer types. More generally, our findings support the notion that hereditary germline variants in the same gene can positively or negatively affect future progression and survival outcomes and responsiveness to therapy in a common human malignancy.

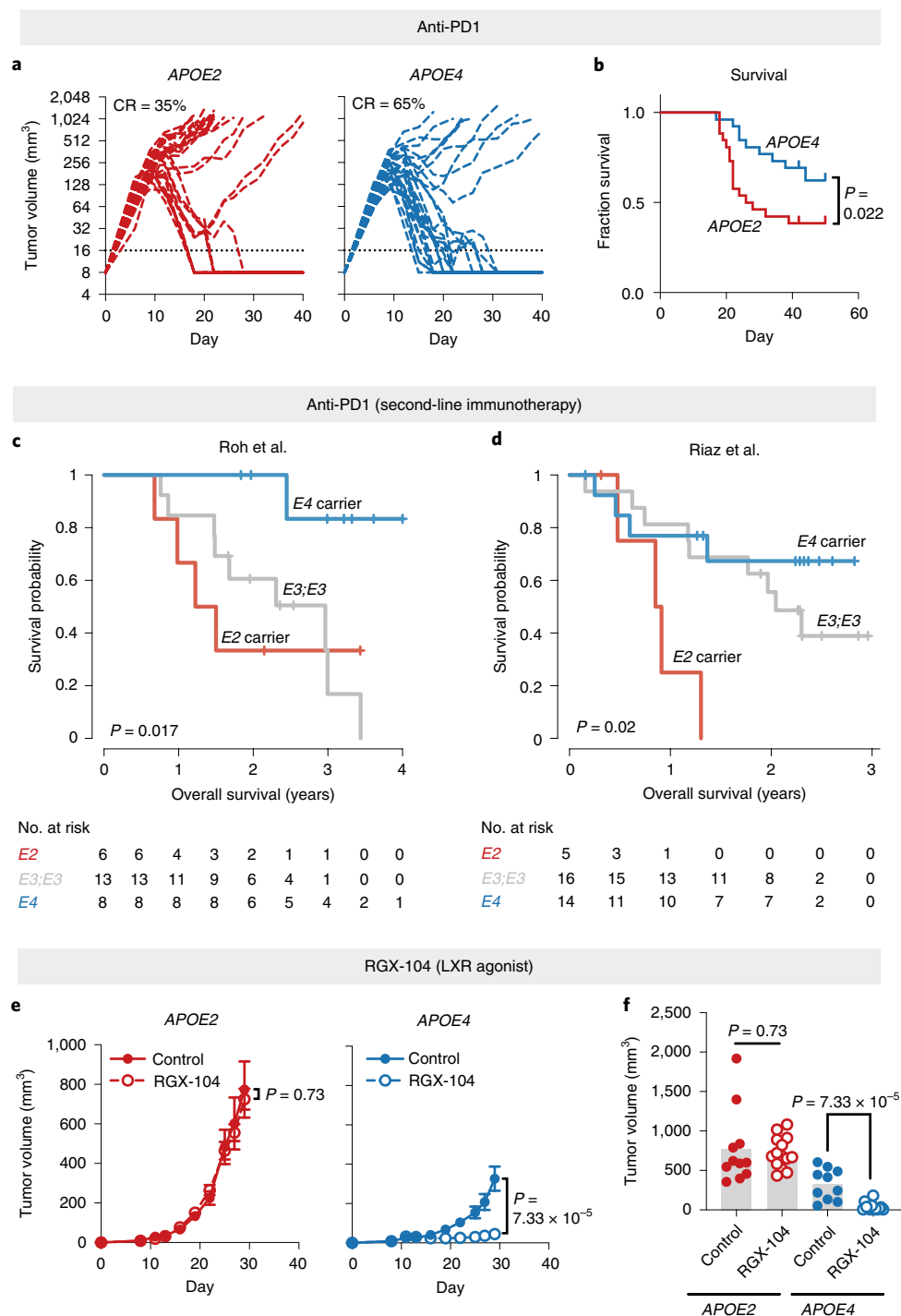


Fig. 4 | APOE genotype modulates melanoma progression in the context of immunotherapy. a, b, Tumor growth (a) and survival (b) of human APOE knock-in mice injected with YUMMER1.7 tumors and treated with anti-PD1 antibody ($n = 26$ per group; $P = 0.022$, two-tailed log-rank test; data pooled from two independent experiments). **c, d**, Survival of patients with melanoma treated with anti-PD1 immunotherapy after failing anti-CTLA4 treatment in the Roh et al. (c) and Riaz et al. (d) studies stratified by APOE carrier status (P values according to two-sided log-rank tests). **e**, Effect of LXR-agonistic treatment on growth of YUMMER1.7 tumors in human APOE knock-in mice ($n = 11, 14, 10$ and 13 for APOE2/ctrl, APOE2/RGX-104, APOE4/ctrl and APOE4/RGX-104 groups, respectively; graphs represent mean values \pm s.e.m., two-tailed t -test; representative of two independent experiments). **f**, Individual tumor volume on day 29 after injection from e. CR, complete remission.

Online content

Any methods, additional references, Nature Research reporting summaries, source data, extended data, supplementary information, acknowledgements, peer review information; details of author contributions and competing interests; and statements of data and

code availability are available at <https://doi.org/10.1038/s41591-020-0879-3>.

Received: 24 January 2020; Accepted: 9 April 2020; Published online: 25 May 2020

References

- Strittmatter, W. J. et al. Apolipoprotein E: high-avidity binding to beta-amyloid and increased frequency of type 4 allele in late-onset familial Alzheimer disease. *Proc. Natl Acad. Sci. USA* **90**, 1977–1981 (1993).
- Corder, E. H. et al. Protective effect of apolipoprotein E type 2 allele for late onset Alzheimer disease. *Nat. Genet* **7**, 180–184 (1994).
- Mahley, R. W. Apolipoprotein E: from cardiovascular disease to neurodegenerative disorders. *J. Mol. Med.* **94**, 739–746 (2016).
- Tavazoie, M. F. et al. LXR/ApoE activation restricts innate immune suppression in cancer. *Cell* **172**, 825–840 (2018).
- Shi, Y. & Holtzman, D. M. Interplay between innate immunity and Alzheimer disease: APOE and TREM2 in the spotlight. *Nat. Rev. Immunol.* **18**, 759–772 (2018).
- Chen, J., Li, Q. & Wang, J. Topology of human apolipoprotein E3 uniquely regulates its diverse biological functions. *Proc. Natl Acad. Sci. USA* **108**, 14813–14818 (2011).
- Weisgraber, K. H., Innerarity, T. L. & Mahley, R. W. Abnormal lipoprotein receptor-binding activity of the human E apoprotein due to cysteine-arginine interchange at a single site. *J. Biol. Chem.* **257**, 2518–2521 (1982).
- Kowal, R. C. et al. Opposing effects of apolipoproteins E and C on lipoprotein binding to low density lipoprotein receptor-related protein. *J. Biol. Chem.* **265**, 10771–10779 (1990).
- Xian, X. et al. Reversal of ApoE4-induced recycling block as a novel prevention approach for Alzheimer's disease. *eLife* **7**, e40048 (2018).
- Kulminski, A. M. et al. Age, gender, and cancer but not neurodegenerative and cardiovascular diseases strongly modulate systemic effect of the apolipoprotein E4 allele on lifespan. *PLoS Genet.* **10**, e1004141 (2014).
- Anand, R., Prakash, S. S., Veeramanikandan, R. & Kirubakaran, R. Association between apolipoprotein E genotype and cancer susceptibility: a meta-analysis. *J. Cancer Res. Clin. Oncol.* **140**, 1075–1078 (2014).
- Pencheva, N. et al. Convergent multi-miRNA targeting of ApoE drives LRP1/LRP8-dependent melanoma metastasis and angiogenesis. *Cell* **151**, 1068–1082 (2012).
- Pencheva, N., Buss, C. G., Posada, J., Merghoub, T. & Tavazoie, S. F. Broad-spectrum therapeutic suppression of metastatic melanoma through nuclear hormone receptor activation. *Cell* **156**, 986–1001 (2014).
- Sullivan, P. M. et al. Targeted replacement of the mouse apolipoprotein E gene with the common human APOE3 allele enhances diet-induced hypercholesterolemia and atherosclerosis. *J. Biol. Chem.* **272**, 17972–17980 (1997).
- Sullivan, P. M., Mezdour, H., Quarfordt, S. H. & Maeda, N. Type III hyperlipoproteinemia and spontaneous atherosclerosis in mice resulting from gene replacement of mouse Apoe with human Apoe*2. *J. Clin. Invest.* **102**, 130–135 (1998).
- Knouff, C. et al. Apo E structure determines VLDL clearance and atherosclerosis risk in mice. *J. Clin. Invest.* **103**, 1579–1586 (1999).
- Wang, J. et al. UV-induced somatic mutations elicit a functional T cell response in the YUMMER1.7 mouse melanoma model. *Pigment Cell Melanoma Res.* **30**, 428–435 (2017).
- Bonacina, F. et al. Myeloid apolipoprotein E controls dendritic cell antigen presentation and T cell activation. *Nat. Commun.* **9**, 3083 (2018).
- Toledo, A., Monzón, J. D., Coleman, J. L., Garcia-Monco, J. C. & Benach, J. L. Hypercholesterolemia and ApoE deficiency result in severe infection with Lyme disease and relapsing-fever *Borrelia*. *Proc. Natl Acad. Sci. USA* **112**, 5491–5496 (2015).
- Shi, Y. et al. ApoE4 markedly exacerbates tau-mediated neurodegeneration in a mouse model of tauopathy. *Nature* **549**, 523–527 (2017).
- Krasemann, S. et al. The TREM2-APOE pathway drives the transcriptional phenotype of dysfunctional microglia in neurodegenerative diseases. *Immunity* **47**, 566–581 (2017).
- The Cancer Genome Atlas Network. Genomic classification of cutaneous melanoma. *Cell* **161**, 1681–1696 (2015).
- Blair, C. K. et al. APOE genotype and cognitive decline in a middle-aged cohort. *Neurology* **64**, 268–276 (2005).
- Deelen, J. et al. A meta-analysis of genome-wide association studies identifies multiple longevity genes. *Nat. Commun.* **10**, 3669 (2019).
- Liu, J. et al. An integrated TCGA pan-cancer clinical data resource to drive high-quality survival outcome analytics. *Cell* **173**, 400–416 (2018).
- Amos, C. I. et al. Genome-wide association study identifies novel loci predisposing to cutaneous melanoma. *Hum. Mol. Genet.* **20**, 5012–5013 (2011).
- Larkin, J. et al. Five-year survival with combined nivolumab and ipilimumab in advanced melanoma. *N. Engl. J. Med.* **381**, 1535–1546 (2019).
- Leach, D. R., Krummel, M. F. & Allison, J. P. Enhancement of antitumor immunity by CTLA-4 blockade. *Science* **271**, 1734–1736 (1996).
- Okazaki, T. & Honjo, T. PD-1 and PD-1 ligands: from discovery to clinical application. *Int. Immunol.* **19**, 813–824 (2007).
- Roh, W. et al. Integrated molecular analysis of tumor biopsies on sequential CTLA-4 and PD-1 blockade reveals markers of response and resistance. *Sci. Transl. Med.* **9**, eaah3560 (2017).
- Riaz, N. et al. Tumor and microenvironment evolution during immunotherapy with nivolumab. *Cell* **171**, 934–949 (2017).
- Evans, R. M. & Mangelsdorf, D. J. Nuclear receptors, RXR, and the Big Bang. *Cell* **157**, 255–256 (2014).
- Hong, C. & Tontonoz, P. Liver X receptors in lipid metabolism: opportunities for drug discovery. *Nat. Rev. Drug Discov.* **13**, 433–444 (2014).
- Nathan, B. P. et al. Differential effects of apolipoproteins E3 and E4 on neuronal growth in vitro. *Science* **264**, 850–852 (1994).

Publisher's note Springer Nature remains neutral with regard to jurisdictional claims in published maps and institutional affiliations.

© The Author(s), under exclusive licence to Springer Nature America, Inc. 2020

Methods

Animal studies. All animal experiments were conducted in accordance with a protocol approved by the Institutional Animal Care and Use Committee at The Rockefeller University. Human *APOE2* (strain no. 1547), *APOE3* (strain no. 1548) and *APOE4* (strain no. 1549) targeted-replacement (knock-in) mice were obtained from Taconic Biosciences. C57BL/6J mice (no. 000664) were obtained from The Jackson Laboratory.

Cell lines. YUMM1.7 cells, originally derived from a *Braf^{V600E/+};Pten^{-/-};Cdkn2a^{-/-}* mouse melanoma model, and their more immunogenic derivative YUMMER1.7 were generously provided by Marcus Bosenberg^{17,35}. Mouse B16F10 melanoma cells, YUMM3.3 melanoma cells (*Braf^{V600E/+};Cdkn2a^{-/-}*) and human umbilical vein endothelial cells (HUVECs) were obtained from the American Tissue Type Collection and cultured according to the supplier's conditions. B16F10 cells transduced with a retroviral construct to express luciferase³⁶ and short hairpin RNA (shRNA) targeting murine *ApoE* (shRNA clone TRCN0000011799; B16F10-TR-shApoE) were described previously¹³. MeWo melanoma cells were originally obtained from the American Tissue Type Collection. The highly metastatic MeWo-LM2 subclone was described previously¹². B16F10 and MeWo-LM2 cells were cultured in DMEM medium with pyruvate and glutamine (11995, Gibco) supplemented with 10% fetal bovine serum (FBS) (F4135, Sigma), penicillin–streptomycin (15140, Gibco) and amphotericin B (17-936E, Lonza). YUMM1.7, YUMM3.3 and YUMMER1.7 cells were cultured in DMEM/F-12 medium with L-glutamine and 15 mM HEPES (11330, Gibco) supplemented with 10% FBS, penicillin–streptomycin, amphotericin B and 1% nonessential amino acids (111400, Gibco). Contamination with mycoplasma was ruled out by PCR testing according to standard protocols³⁷.

Tumor growth studies and treatments. To assess the effect of *APOE* genotype on the growth of syngeneic melanoma, we subcutaneously injected 1×10^5 YUMM1.7 or YUMM3.3 cells into the flank of 6–10-week-old, sex-matched human *APOE* targeted-replacement mice. Cells were injected in a total volume of 100 μ l, and YUMM1.7 cells were mixed 1:1 with growth-factor-reduced Matrigel (356231, Corning) before injection. Tumor size was measured on the indicated days using digital calipers, and tumor volume was calculated as (small diameter)² \times (large diameter) \times π / 6. In experiments employing YUMMER1.7 cells, 5×10^5 cells resuspended in phosphate-buffered saline (PBS) were injected subcutaneously into the flank. The sex of the mice for experiments with YUMM1.7, YUMM3.3 and B16F10 cells was matched to the sex of the tumor cell line (males for YUMM1.7 and B16F10, females for YUMM3.3). YUMMER1.7 cells were injected into female mice.

To deplete T cells in vivo, 400 μ g each of anti-CD4 (Bio X Cell, clone GK1.5) and anti-CD8 (Bio X Cell, clone 53-6.7) antibodies were injected intraperitoneally on days 7, 14 and 21 after tumor cell injection. Control mice received PBS injections on the same days. Efficient depletion was verified by flow cytometry on day 27 after tumor injection. For LXR-agonistic treatment, mice were administered chow supplemented with the synthetic LXR-agonist RGX-104 (Rgenix⁴) at 628.5 mg kg⁻¹ (Research Diets, approximate target dose of 100 mg kg⁻¹ body weight) starting on day 3 after injection. For anti-PD1 treatment, mice were injected intraperitoneally with 250 μ g and 125 μ g of anti PD-1 antibody (Bio X Cell, clone RMP1-14) on days 6 and 9 after tumor cell injection, respectively. Control mice received PBS injections on the same days. For survival analysis in the YUMMER1.7 model, mice were euthanized when the tumor volume exceeded 1,000 mm³. Therapy responses were considered complete (CR, complete response) when tumor volumes fell below 16 mm³ (lowest limit of detection).

Tail vein metastasis assays. For tail vein assays, B16F10-shApoE cells stably expressing a retroviral construct encoding luciferase were used to assess cancer progression by bioluminescence imaging as described previously¹³. Because our previous work demonstrated that tumor-derived APOE significantly modulates progression in the metastatic but not in the primary tumor site^{12,13}, we silenced tumoral *ApoE* expression in B16F10 cells employed in tail vein assays using RNA interference. To assess whether *APOE* genotype affects metastatic progression, 1×10^5 cells were resuspended in 100 μ l of PBS and injected into the tail vein of 6–8-week-old male human *APOE* knock-in mice. Bioluminescence imaging was performed approximately twice a week, and the signal was normalized to the signal obtained on day 0.

Mouse genotyping. Genotyping to distinguish between mouse and human *APOE* was performed using standard PCR with independent reactions for mouse and human *APOE* (PCR product lengths of 200 bp and approximately 600 bp, respectively). To distinguish between human *APOE* alleles, we used PCR-based restriction fragment length polymorphism genotyping³⁸. In brief, a 244-bp fragment of *APOE* was amplified using standard PCR and digested with HhaI (R0139S, New England Biolabs), and allele-specific products were resolved on a 15% polyacrylamide gel. The following primers were used for the indicated PCR reactions:

Mouse versus human knock-in *APOE* mice
Common forward: 5'-TAC CGG CTC AAC TAG GAA CCA T-3'

Mouse *ApoE* reverse: 5'-TTT AAT CGT CCT CCA TCC CTG C-3'
Human *APOE* reverse: 5'-GTT CCA TCT CAG TCC CAG TCTC-3'
Human *APOE* allele restriction length polymorphism
Human *APOE* forward: 5'-ACA GAA TTC GCC CCG GCC TGG TAC AC-3'
Human *APOE* reverse: 5'-TAA GCT TGG CAC GGC TGT CCA AGG A-3'

Hematopoietic stem cell transplantation. Six-to-7-week-old C57BL/6J mice were whole-body irradiated with 10.5 Gray (two doses of 525 rad each 3.5 h apart). Six hours after the last dose of irradiation, $2-3 \times 10^6$ nucleated bone marrow cells isolated from 6–8-week-old *APOE* knock-in mice ($n = 5$ per group) were infused into recipient mice by retroorbital injection. Bone marrow chimeras were reconstituted for 8 weeks before experimental use.

Quantitative real-time PCR. Total RNA from cells cultured in triplicate was isolated with the Total RNA Purification Kit (17200, Norgen Biotek). The SuperScript III First-Strand Synthesis System (18080051, Thermo Fisher) was used to reverse transcribe 1 μ g of total RNA into cDNA according to the manufacturer's instructions using oligo(dT) primers. Subsequently, quantitative real-time PCR was performed using Fast SYBR Green Master Mix (Applied Biosystems) and an Applied Biosystems 7900HT system. Expression of *ApoE* was normalized to *Gapdh* expression for each sample. Primer sequences were as follows:

ApoE forward: 5'-CTG ACA GGA TGC CTA GCC G-3'
ApoE reverse: 5'-CGC AGG TAA TCC CAG AAG C-3'
Gapdh forward: 5'-GCA CAG TCA AGG CCG AGA AT-3'
Gapdh reverse: 5'-GCC TTC TCC ATG GTG GTG AA-3'

Isolation of tumor-infiltrating leukocytes. To isolate tumor-infiltrating leukocytes, YUMM1.7 tumors were resected on day 21 after injection and thoroughly minced on ice using scalpels. Tumor pieces were incubated in HBSS2⁻ (HBSS with calcium and magnesium (24020, Gibco) supplemented with 2% FBS, 1 mM sodium pyruvate (11360, Gibco), 25 mM HEPES (15630, Gibco), 500 U ml⁻¹ collagenase IV (LS004188, Worthington), 100 U ml⁻¹ collagenase I (LS004196, Worthington) and 0.2 mg ml⁻¹ DNase I (10104159001, Roche)) for 30 min at 37 °C on an orbital shaker (80 r.p.m.). After thorough trituration, the mixture was passed through a 70- μ m strainer and diluted with HBSS2⁻ (HBSS without calcium and magnesium (14170, Gibco), 2% FBS, 1 mM sodium pyruvate and 25 mM HEPES). After centrifugation, the cell pellet was resuspended in a 35% Percoll solution (170891, GE Healthcare), and a phase of 70% Percoll was underlaid using a glass Pasteur pipette. The resulting gradient was centrifuged at 800g for 20 min at room temperature without brakes. After removal of the red blood cell-containing pellet on the bottom and excess buffer-containing cellular debris on the top, the cell population at the Percoll interphase enriched for tumor-infiltrating leukocytes was washed twice with HBSS2⁻.

Flow cytometry. Unless otherwise mentioned, all steps were performed on ice and under protection from light. Fc receptors were blocked by incubation with 2.5 μ g ml⁻¹ anti-CD16/32 antibody (clone 93; 101320, BioLegend) in staining buffer (25 mM HEPES, 2% FBS, 10 mM EDTA (351-027, Quality Biological) and 0.1% sodium azide (7144.8-16, Ricca) in PBS) for 10 min. Cells were incubated with antibodies diluted in staining buffer for 20 min, washed with PBS, incubated with Zombie NIR Fixable Live/Dead Stain (423105, BioLegend) for 20 min at room temperature and washed twice with staining buffer. Cells were analyzed on an LSR Fortessa (BD Biosciences). For cell quantification, CountBright counting beads (C36950, Thermo Fisher) were added to the samples before analysis. For compensation, single-color controls with UltraComp beads (01-2222-42, Thermo Fisher) for antibodies and amine-reactive beads (A10628, Thermo Fisher) for Zombie live/dead stain were used.

For intracellular staining of cytokines, cells were incubated with 500 ng ml⁻¹ ionomycin (I0634, Sigma), 100 ng ml⁻¹ phorbol 12-myristate 13-acetate (P8139, Sigma) and 10 μ g ml⁻¹ brefeldin A (B7651, Sigma) for 3–4 h at 37 °C before surface labeling and live/dead staining as described above. Cells were then incubated in fixation/permeabilization buffer (00-5523, eBioscience) for 30 min, washed with permeabilization buffer (00-5523, eBioscience) and incubated with antibodies diluted in permeabilization buffer for 20 min. Finally, cells were washed with permeabilization buffer and subsequently with staining buffer.

scRNA-seq of tumor-infiltrating leukocytes. Human *APOE* knock-in mice ($n = 6$ per group) were subcutaneously injected with 1×10^5 YUMM1.7 cells on the flank (mixed 1:1 with growth-factor-reduced Matrigel (356231, Corning)). Tumors were resected on day 19 after injection, and tumor-infiltrating leukocytes were isolated as outlined above. Fc receptors were blocked with anti-CD16/32 antibody (clone 93; 101320 BioLegend), and cells were stained with an anti-CD45 antibody and DAPI in flow cytometry buffer without sodium azide. Subsequently, 10,000 CD45⁺ DAPI⁻ leukocytes from each mouse were independently sorted on a BD FACSAria II cell sorter, and samples from the same genotype were pooled (i.e. total of 60,000 cells per genotype). Next, 5,000 cells per genotype were targeted for scRNAseq on a Chromium Single Cell System (10 \times Genomics). Samples were processed as per the manufacturer's instructions (chromium single-cell 3' reagents, v3 chemistry), and libraries were sequenced on an Illumina NextSeq sequencer.

Pre-processing of sequencing results to generate transcript matrices was performed using the 10× Genomics Cell Ranger pipeline with default settings (v3.0.1). Further downstream analysis was performed in R using the Seurat package (v3.0.2). Cells were excluded if fewer than 200 or more than 6,000 genes were detected or if mitochondrial transcripts accounted for more than 10% of reads; genes were excluded if they were detected in fewer than five cells. The two data sets were integrated using Seurat's default settings, resulting in an expression matrix of 10,050 cells by 15,495 genes. Data were scaled and principal component analysis was performed using Seurat's default settings. Cells were clustered using the FindNeighbors (20 dimensions of reduction) and FindClusters functions at default settings; uniform manifold approximation and projection (UMAP) was calculated for visualizing clusters. Differential gene expression analysis between each cluster was performed using a Wilcoxon rank-sum test. The identity of cell clusters was determined by cross-referencing top differentially expressed transcripts with the Immunological Genome Project³⁹ (Extended Data Fig. 3a). The identity of one cell cluster remained ambiguous, and further subclustering revealed the presence of a mixed population (data not shown), prompting us to label this cluster as 'diverse'.

For gene set enrichment analysis (GSEA), differential expression of genes between *APOE4* and *APOE2* for each cluster was calculated using a Wilcoxon rank-sum test, and genes were ranked using the metric $[-\log_{10}(P \text{ value})]/[\text{sign of log-fold change}]$. The ranked gene list was used for calculating GSEA using the clusterProfiler package with the Hallmark gene sets in the MSigDB database^{40,41}. For visualization, the number of clusters with significant enrichment was plotted for pathways that were significant in more than three clusters. For lineage summarization, all macrophage, monocyte, MDSC, basophil and mast cell clusters were grouped as 'myeloid'; T cell, B cell and NK clusters were grouped as 'lymphoid'; all DC clusters were grouped as 'DCs'; and the remaining clusters were grouped as 'other'.

Antibodies. The following anti-mouse fluorophore-conjugated antibodies were used for flow cytometry: CD45-BV785 (clone: 30-F11, cat. no. 103149, supplier: BioLegend, dilution: 1:3,000), B220-BUV395 (RA3-6B2, 563793, BD Biosciences, 1:400), CD11b-BV605 (M1/70, 101257, BioLegend, 1:6,000), CD11b-FITC (M1/70, 101206, BioLegend, 1:4,000), Ly6G-PerCP/Cy5.5 (1A8, 127616, BioLegend, 1:500), Ly6C-BV711 (HK1.4, 128037, BioLegend, 1:12,000), I-A/I-E-BV421 (M5/114.15.2, 107632, BioLegend, 1:9,000), F4/80-FITC (BM8, 123108, BioLegend, 1:500), CD24-PE (M1/69, 101808, BioLegend, 1:5,000), CD103-APC (2E7, 121414, BioLegend, 1:500), CD19-FITC (1D3/CD19, 152404, BioLegend, 1:1,500), TCRβ-PerCP/Cy5.5 (H57-597, 109228, BioLegend, 1:200), CD49b-APC (HMa2, 103516, BioLegend, 1:300), CD4-BV605 (GK1.5, 100451, BioLegend, 1:200), CD8α-AF700 (53-6.7, 100730, BioLegend, 1:1,000), Granzyme B-PE (QA16A02, 372208, BioLegend, 1:200) and IFNγ-PE/Cy7 (XMG1.2, 25-7311-82, eBioscience, 1:500).

Immunofluorescence microscopy. YUMM1.7 tumors were excised and fixed in 4% paraformaldehyde at 4 °C for 24 h. Fixed tumors were embedded in paraffin and sectioned in 5-μm-thick slices. Sections were dewaxed and rehydrated by incubation with xylene and descending ethanol concentrations. Antigen retrieval was performed by microwaving samples in citrate buffer (C9999, Sigma) for 30 min. Samples were blocked by incubation with 5% goat serum in PBS with 0.1% Tween-20 (PBST) for 1 h. Subsequently, the sections were stained with anti-endomucin (clone V.7C7, Santa Cruz Biotechnology; 1:200 in PBST with 5% goat serum) or anti-CD8 antibody (rabbit polyclonal, Synaptic Systems, 1:200 in PBST with 5% goat serum) at 4 °C overnight. Slides were washed three times with PBS and stained with AF555-conjugated anti-rat or AF488-conjugated anti-rabbit antibody (1:200 in PBST, Thermo Fisher Scientific) for 45 min. Slides were washed with PBS and nuclei were counterstained with DAPI (2.5 μg ml⁻¹, Roche) before mounting with Prolong Gold (Thermo Fisher Scientific). Images of tumor sections were acquired using an RS-G4 confocal microscope (Caliber I.D.). Images were quantified using CellProfiler (v3.1.8). Four sections per tumor were analyzed and averaged. Samples without addition of primary antibody served as negative controls.

Matrigel invasion assay. The assay was performed similarly to as described previously¹². B16F10-TR-shApoe mouse melanoma cells were serum starved overnight in DMEM supplemented with 0.2% FBS. Before starting the assay, four Matrigel invasion chambers per condition (Corning, 354480) were equilibrated at 37 °C with 500 μl of 0.2% FBS DMEM in the top and bottom chambers. After 30 min, the starvation medium in the top chamber was removed and replaced with 500 μl of starvation medium containing 1×10^5 melanoma cells and either 10 μg ml⁻¹ of recombinant APOE2 or APOE4 (Tonbo Biosciences 21-9195 and 21-9190) or an equimolar concentration of bovine serum albumin (BSA) (20 μg ml⁻¹, Sigma A3059). Chambers were then kept at 37 °C for 24 h to allow for invasion. Subsequently, the chambers were washed with 1× PBS, the tops were scraped with cotton swabs to remove residual noninvading cells and the inserts were fixed in 4% paraformaldehyde for 20 min. After washing again with PBS, inserts were stained with DAPI (Roche, 10236276001) for 5 min, cut out and then mounted bottom-up on slides with ProLong Gold Antifade Mountant (Invitrogen, P36930).

Four representative images per insert were taken using a Zeiss Axiovert 40 CFL fluorescence microscope at ×10 magnification, and the number of invaded cells was quantified.

Endothelial recruitment assay. HUVECs were serum starved overnight in EGM-2 media (Lonza, CC-3162) containing 0.2% FBS. Concurrently, 5×10^4 highly metastatic MeWo-LM2 human melanoma cells were plated in a 24-well plate in DMEM supplemented with 10% FBS. On the day of the assay, the medium was replaced with EGM-2 starvation medium, and Mewo-LM2 cells were allowed to enrich the media for 6–8 h at 37 °C. Subsequently, BSA (20 μg ml⁻¹, Sigma, A3059), APOE2 or APOE4 (10 μg ml⁻¹, Tonbo Biosciences, 21-9195 and 21-9190) were added to the media, and 3.0-μm PET membrane inserts (Falcon, 353492) were placed in the wells. HUVECs were trypsinized, resuspended and seeded equally into the top chambers. The cells were allowed to migrate for 16–18 h, after which the inserts were mounted and analyzed as described for the invasion assay above.

Analysis of APOE genotype in the TCGA-SKCM study. To assess *APOE* genotype in patients with melanoma from the TCGA-SKCM study, we downloaded aligned whole-exome sequencing BAM files sliced for the genomic coordinates chr19:44904748-44910394 (GRCh38) using the Genomic Data Commons API²². We called *APOE* variants using the samtools/bcftools package, providing allele frequencies for chr19:44908684 (rs429358) and chr19:44908822 (rs7412) as determined in the Atherosclerosis Risk in Communities (ARIC) study²³ as a prior distribution. Normal tissue samples (blood, solid tissue or buccal cells) were available for 470 patients. No genotype could be determined in ten patients. Additionally, patients who exhibited the *APOE2*/*APOE4* heterozygous genotype ($n = 5$) were excluded from analyses except for genotype frequency assessment. *APOE* genotype abundance in the normal population was based on the assessment of Caucasian patients in the ARIC study.

Clinical data, including survival times and clinical response, were used as recently curated²⁵. The R package 'TCGAbiolinks' was used to add clinical data for Breslow depth and Clark level. To assess the effect of *APOE* genotype on survival, Kaplan–Meier survival analyses were performed, and statistical significance was assessed with the log-rank test using the 'survival' and 'survminer' packages. HRs were calculated according to a Cox proportional hazard regression model using the 'survival' R package. For multivariable analysis, variables found to be significantly associated with survival in univariate analysis were tested for significance in a multivariable Cox proportional hazard model. For visualization purposes, survival data were truncated at 12 years. Given the sample sizes in the TCGA data set, our analyses had greater than 80% power to detect an HR of approximately 1.4 or larger, assuming a type I error of 5%. All analyses were performed using R v3.5 (The R Foundation for Statistical Computing) and RStudio v1.1.3.

Analysis of APOE genotype in the MDACC melanoma study. GWAS genotyping results of the MDACC melanoma study²⁶ were downloaded from dbGap, and the *APOE* variant-defining single-nucleotide polymorphisms rs429358 and rs7412 were selected using Plink. Genotyping data were filtered to exclude variants with minor allele frequency less than 1%, genotyping rate less than 95% and departure from the Hardy–Weinberg equilibrium at $P < 1 \times 10^{-6}$. Samples were excluded if the missing genotype call rate exceeded 5%. Genomic coordinates were lifted from genome assembly hg18 to hg19 using the UCSC liftOverPlink utility, and strands were aligned using GenotypeHarmonizer and the 1000 Genomes Project reference genome. Because no individual was found to exhibit the minor allele at rs429358, inadequate genotyping at this locus was assumed as described by others⁴², prompting us to impute the genotype at this locus based on a previously validated approach⁴³ before performing survival analysis (Extended Data Fig. 9a,b). Pre-phasing was performed using Shapelt v2, and variants in the genomic region 19:45411941-45422946 were imputed using Impute2 with parameters as suggested specifically for *APOE* imputation (-NE 20000 -iter 100 -call_thresh 0.8 -align_by_maf_g)⁴². Subsequent analysis of the association between clinical variables and *APOE* genotype was performed as described for the TCGA-SKCM study above.

Analysis of APOE genotype in the anti-PD1 melanoma studies by Riaz et al. and Roh et al. Analyses of the Roh et al.³⁰ and Riaz et al.³¹ studies were performed as described for the TCGA-SKCM study. In brief, normal tissue whole-exome sequencing data were downloaded from dbGaP (BioProject IDs PRJNA369259 and PRJNA359359), and *APOE* genotype was called as detailed above. No genotype could be determined for one patient in the Roh et al. study. For the Roh et al. study, only patients who received both anti-CTLA4 and anti-PD1 treatment were considered. In the Riaz et al. study, patients were stratified by prior CTLA4 treatment status. Kaplan–Meier survival analyses were performed using the 'survival' and 'survminer' packages, as detailed above.

Statistical analysis. Unless otherwise noted, all data are expressed as mean ± s.e.m. Groups were compared using tests for significance as indicated in the figure legends and the text. A significant difference was concluded at $P < 0.05$.

Reporting Summary. Further information on research design is available in the Nature Research Reporting Summary linked to this article.

Data availability

All data analyzed from published studies are referenced and publicly available under the following accession numbers: TCGA-SKCM, dbGaP accession [p8](https://www.ncbi.nlm.nih.gov/geo/query/acc.cgi?acc=GSE146613); MDACC GWAS study, [p1](https://www.ncbi.nlm.nih.gov/geo/query/acc.cgi?acc=GSE146613); Roh et al. anti-PD1 treatment study, dbGaP BioProject ID [PRJNA369259](https://www.ncbi.nlm.nih.gov/bioproject/PRJNA369259); and Riaz et al. anti-PD1 treatment study, dbGaP BioProject ID [PRJNA359359](https://www.ncbi.nlm.nih.gov/bioproject/PRJNA359359). scRNA-seq data have been deposited at the Gene Expression Omnibus under accession number [GSE146613](https://www.ncbi.nlm.nih.gov/geo/query/acc.cgi?acc=GSE146613). All other data are available from the corresponding author upon reasonable request.

References

35. Meeth, K., Wang, J. X., Micevic, G., Damsky, W. & Bosenberg, M. W. The YUMM lines: a series of congenic mouse melanoma cell lines with defined genetic alterations. *Pigment Cell Melanoma Res.* **29**, 590–597 (2016).
36. Ponomarev, V. et al. A novel triple-modality reporter gene for whole-body fluorescent, bioluminescent, and nuclear noninvasive imaging. *Eur. J. Nucl. Med. Mol. Imaging* **31**, 740–751 (2004).
37. Young, L., Sung, J., Stacey, G. & Masters, J. R. Detection of mycoplasma in cell cultures. *Nat. Protoc.* **5**, 929–934 (2010).
38. Hixson, J. E. & Vernier, D. T. Restriction isotyping of human apolipoprotein E by gene amplification and cleavage with HhaI. *J. Lipid Res.* **31**, 545–548 (1990).
39. Yoshida, H. et al. The cis-regulatory atlas of the mouse immune system. *Cell* **176**, 897–912 (2019).
40. Yu, G., Wang, L. G., Han, Y. & He, Q. Y. clusterProfiler: an R package for comparing biological themes among gene clusters. *OMICS* **16**, 284–287 (2012).
41. Subramanian, A. et al. Gene set enrichment analysis: a knowledge-based approach for interpreting genome-wide expression profiles. *Proc. Natl Acad. Sci. USA* **102**, 15545–15550 (2005).
42. Radmanesh, F. et al. Accuracy of imputation to infer unobserved *APOE* epsilon alleles in genome-wide genotyping data. *Eur. J. Hum. Genet.* **22**, 1239–1242 (2014).

Acknowledgements

We thank members of our laboratory and M. Tavazoie for comments on previous versions of the manuscript. We are grateful for assistance by Rockefeller University resource centers: S. Mazel and staff of the flow cytometry resource center, V. Francis and other veterinary staff of the Comparative Bioscience Center for animal husbandry and

care, C. Zhao and staff at the genomics resource center for assistance with scRNA-seq and A. North and staff at the Bio-Imaging Resource Center. We express gratitude to M. Bosenberg (Yale University) for kindly providing the YUMM1.7 and YUMMER1.7 cell lines. We thank the groups of P. Sullivan and N. Maeda for generating the human *APOE* targeted-replacement mice and making them available through Taconic Biosciences. We are grateful to E. McMillan for early help with whole-exome sequencing analysis. We also thank M. Szarek and H. Mostafavi for statistical advice. This work was supported by National Institutes of Health grant RO1CA184804-01A2 (to S.F.T.). B.N.O. was supported by a Deutsche Forschungsgemeinschaft postdoctoral fellowship (OS 498/1-1). J.B. and K.N.T. were supported by scholarships from the German National Academic Foundation. N.A. was supported by Medical Scientist Training Program grant T32GM007739 from the National Institutes of Health. B.T. was supported by the Lucy Lee Chiles Fellowship from the Hope Funds for Cancer Research. R.D.V. was supported in part by grant UL1 TR001866 from the National Center for Advancing Translational Sciences, National Institutes of Health Clinical and Translational Science Award program. S.F.T. was supported by a Faculty Scholars grant from the Howard Hughes Medical Institute, the Black Family Metastasis Center at Rockefeller University and by the Reem-Kayden award.

Author contributions

B.N.O. and S.F.T. conceived the study, supervised all research and wrote the manuscript. B.N.O., J.B., N.A., K.N.T. and B.T. conducted experiments. B.N.O. analyzed whole-exome sequencing, scRNA-seq and clinical data. R.D.V. provided advice for statistical analysis.

Competing interests

S.F.T. and B.N.O. are inventors on a US provisional patent application encompassing aspects of this work. S.F.T. is a cofounder, shareholder and member of the scientific advisory board of Rgenix.

Additional information

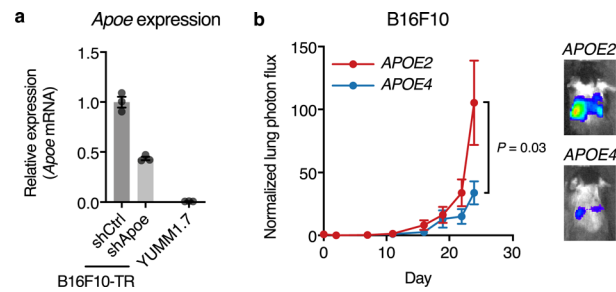
Extended data is available for this paper at <https://doi.org/10.1038/s41591-020-0879-3>.

Supplementary information is available for this paper at <https://doi.org/10.1038/s41591-020-0879-3>.

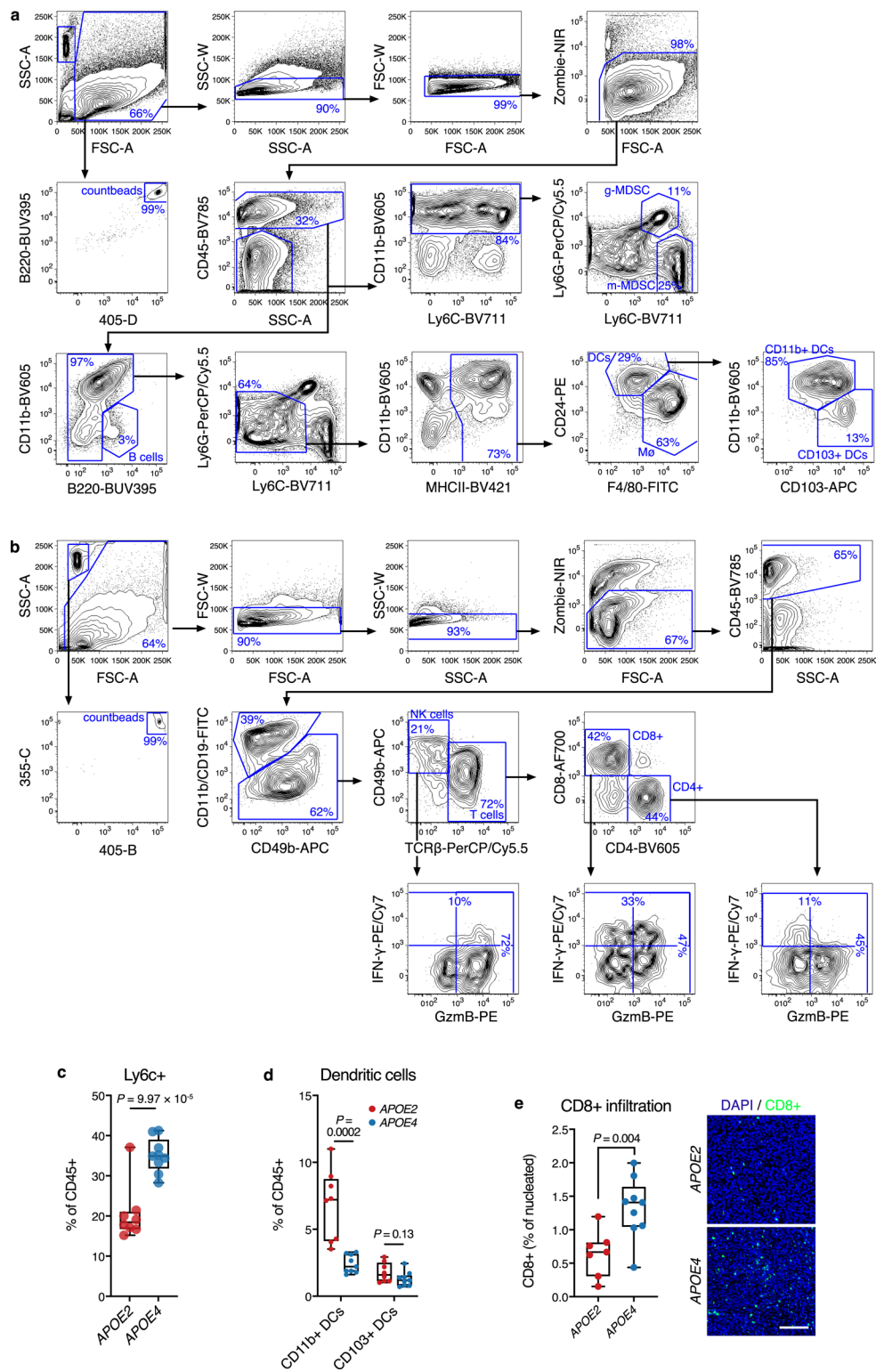
Correspondence and requests for materials should be addressed to S.F.T.

Peer review information Javier Carmona was the primary editor on this article and managed its editorial process and peer review in collaboration with the rest of the editorial team.

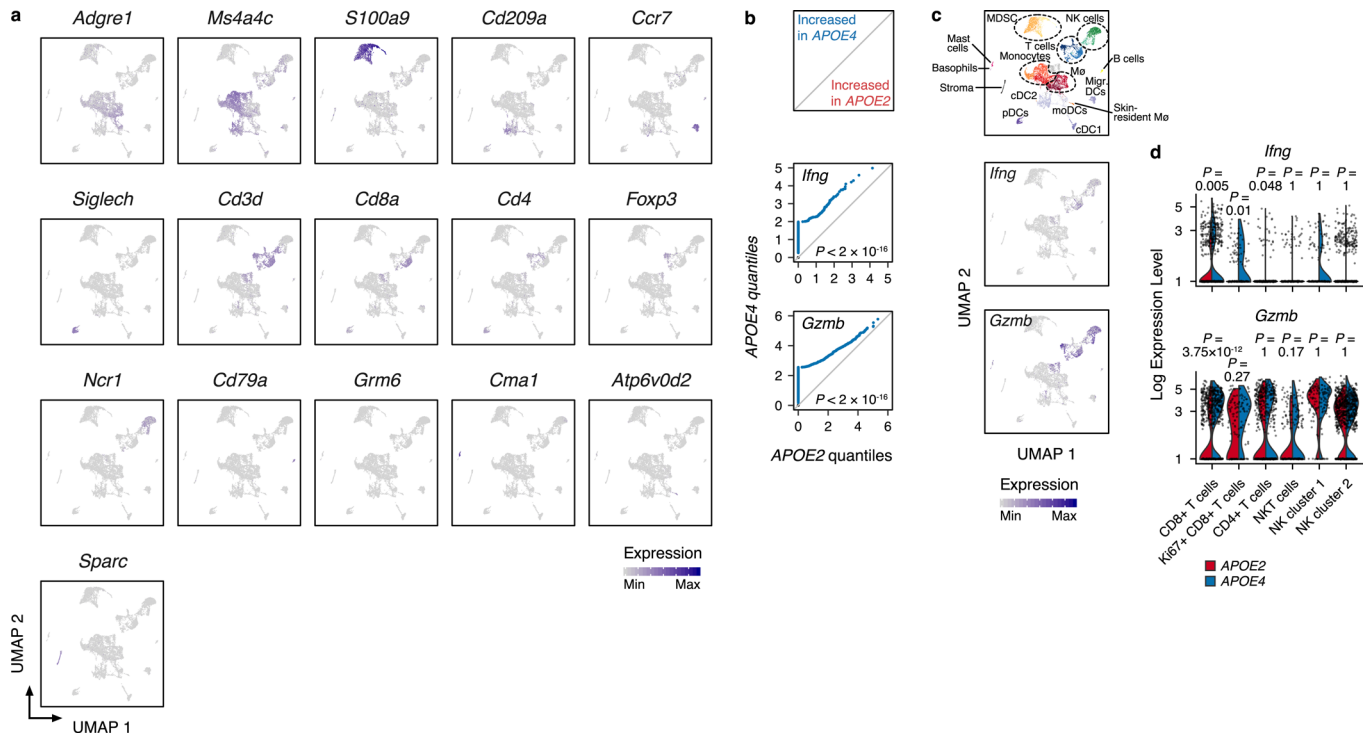
Reprints and permissions information is available at www.nature.com/reprints.



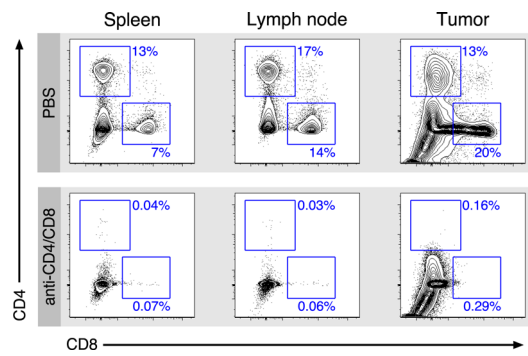
Extended Data Fig. 1 | Human APOE variants modulate metastatic progression of murine melanoma. **a**, Relative expression of murine *Apoe* determined by qRT-PCR in B16F10 cells expressing shCtrl and shApoe hairpins and in YUMM1.7 cells ($n = 3$ cell culture replicates per group, graph represents mean values \pm s.e.m.). **b**, Bioluminescence imaging of metastatic progression of murine melanoma B16F10-TR-shApoe cells intravenously injected into APOE knock-in mice ($n = 10$ mice per group; one-tailed Mann-Whitney test; graph represents mean values \pm s.e.m.; representative of two independent experiments). Images correspond to representative mice on day 24 after injection.



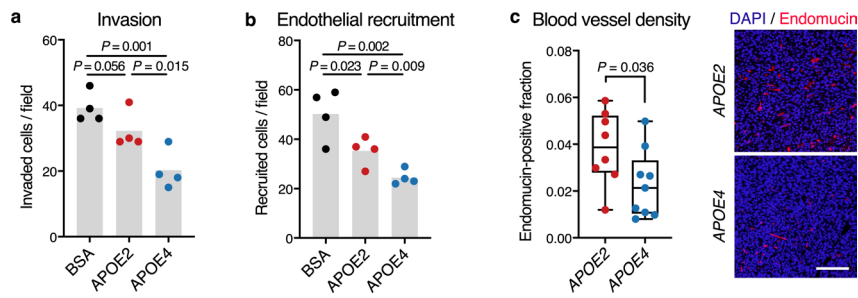
Extended Data Fig. 2 | Immunoprofiling of the tumor microenvironment in *APOE2* versus *APOE4* mice. **a–b**, Representative flow cytometry plots from two independent experiments demonstrating the gating strategy to identify major myeloid (**a**) and lymphoid (**b**) cell subsets in the tumor microenvironment. **c–d**, Proportion of monocytic Ly6c+ (**c**) and dendritic cell (**d**) subsets in the immune microenvironment of YUMM1.7 tumors in *APOE2* and *APOE4* mice ($n = 8$ and 9 mice for *APOE2* and *APOE4*, respectively; representative of two independent experiments). **e**, Intratumoral CD8+ T cell infiltration in YUMM1.7 tumors from *APOE2* and *APOE4* mice ($n = 7$ and 9 mice for *APOE2* and *APOE4* groups, respectively). Images show representative sections (scale bar = $100 \mu\text{m}$). All P values are based on two-tailed t -tests. Box plots show median, first and third quartiles, and whiskers represent minimum and maximum values.



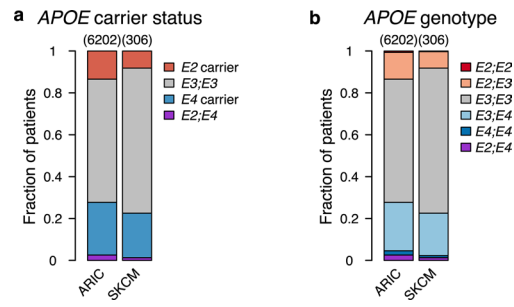
Extended Data Fig. 3 | Extended single cell RNA-sequencing data. **a**, Uniform manifold approximation and projection (UMAP) plots illustrating the distribution of the expression of manually curated, lineage-defining genes. **b**, Paired quantile-quantile plots for the expression of *Ifng* and *Gzmb* in CD45+ cells infiltrating tumors in *APOE2* and *APOE4* mice (P values according to two-sided Wilcoxon rank-sum test). **c**, Uniform manifold approximation and projection (UMAP) plots illustrating the distribution of *Ifng* and *Gzmb* expression across immune cell clusters. **d**, Violin plots showing the distribution of *Ifng* and *Gzmb* expression across T and NK cell subsets from (**b-c**) (P values according to two-sided Wilcoxon rank-sum test adjusted for total number of clusters by FDR; plots extend from minimum to maximum values). A total of 10,050 cells were sequenced ($n = 4,665$ and 5,385 cells for *APOE2* and *APOE4* groups, respectively). Cells were harvested from $n = 6$ biologically averaged mice for each group.



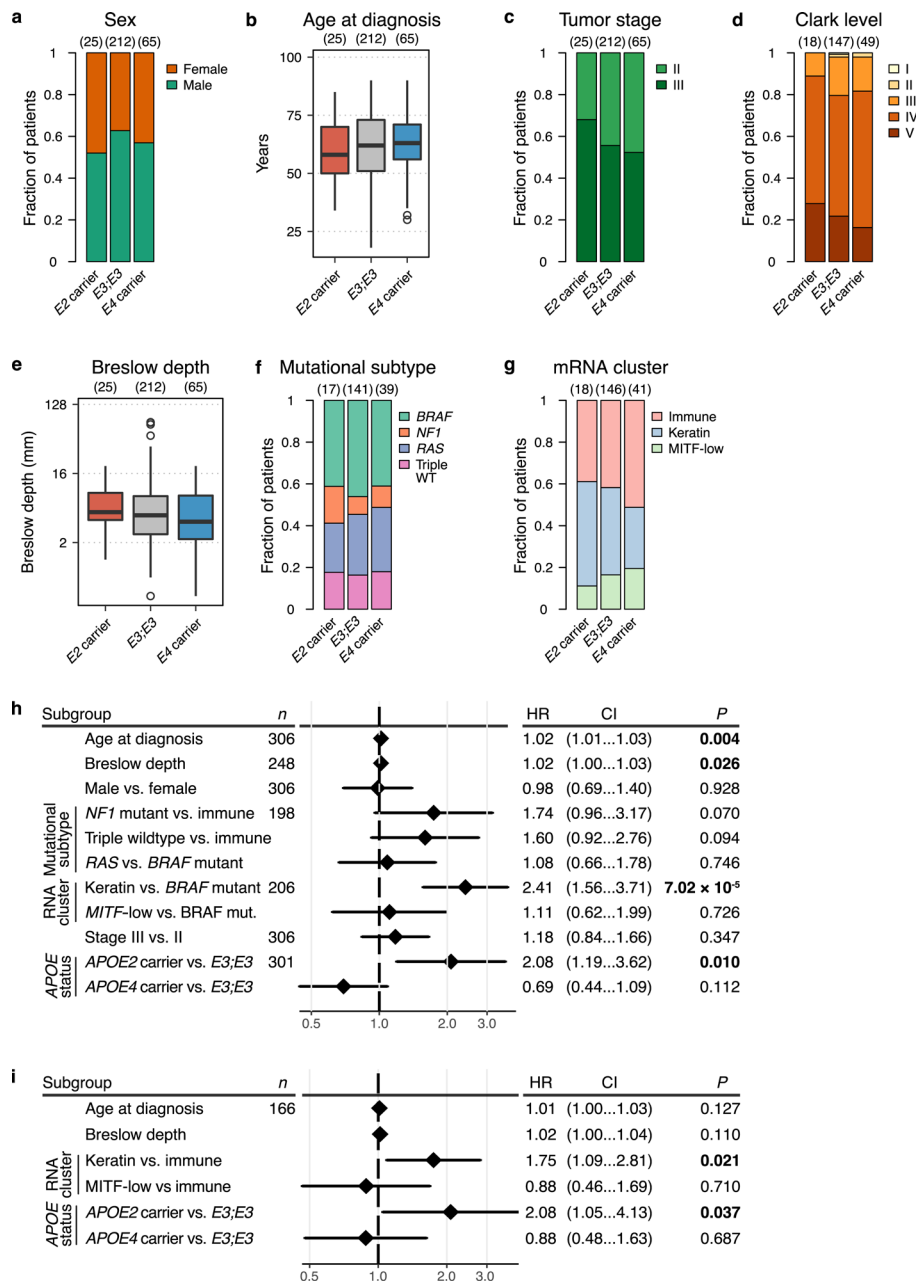
Extended Data Fig. 4 | Efficiency of in-vivo T cell depletion. Representative flow cytometry plots of two independent experiments of samples from spleens, lymph nodes, and tumors of mice treated with PBS versus anti-CD4 and anti-CD8 antibodies.



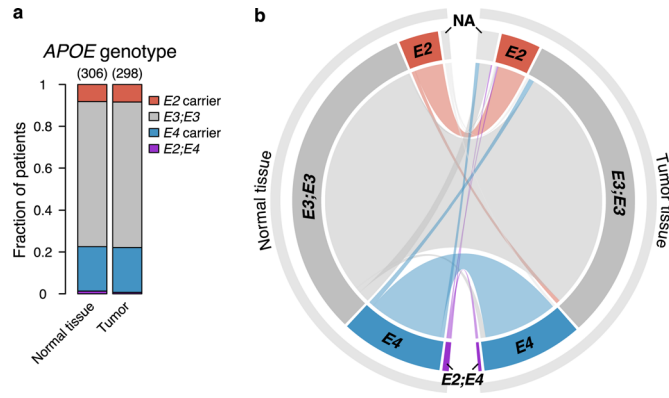
Extended Data Fig. 5 | APOE variants differentially impact cancer cell invasion and endothelial recruitment. **a**, Matrigel invasion by 1×10^5 mouse melanoma B16F10-TR-shApoE cells treated with the indicated recombinant proteins ($n = 4$ biologically independent samples; one tailed t-test). **b**, Trans-well recruitment of 1×10^5 human umbilical vein endothelial cells treated with the indicated recombinant proteins by 5×10^4 human melanoma MeWo-LM2 cells ($n = 4$ biologically independent samples; one tailed t-tests). Data in **(a-b)** are representative of three independent experiments. **c**, Blood vessel density in YUMM1.7 tumors from *APOE2* and *APOE4* mice ($n = 8$ and 9 mice for *APOE2* and *APOE4* groups, respectively; two-tailed Mann-Whitney test; box plots show median, first and third quartiles, and whiskers represent minimum and maximum values.). Images show representative sections (scale bar = $100 \mu\text{m}$).



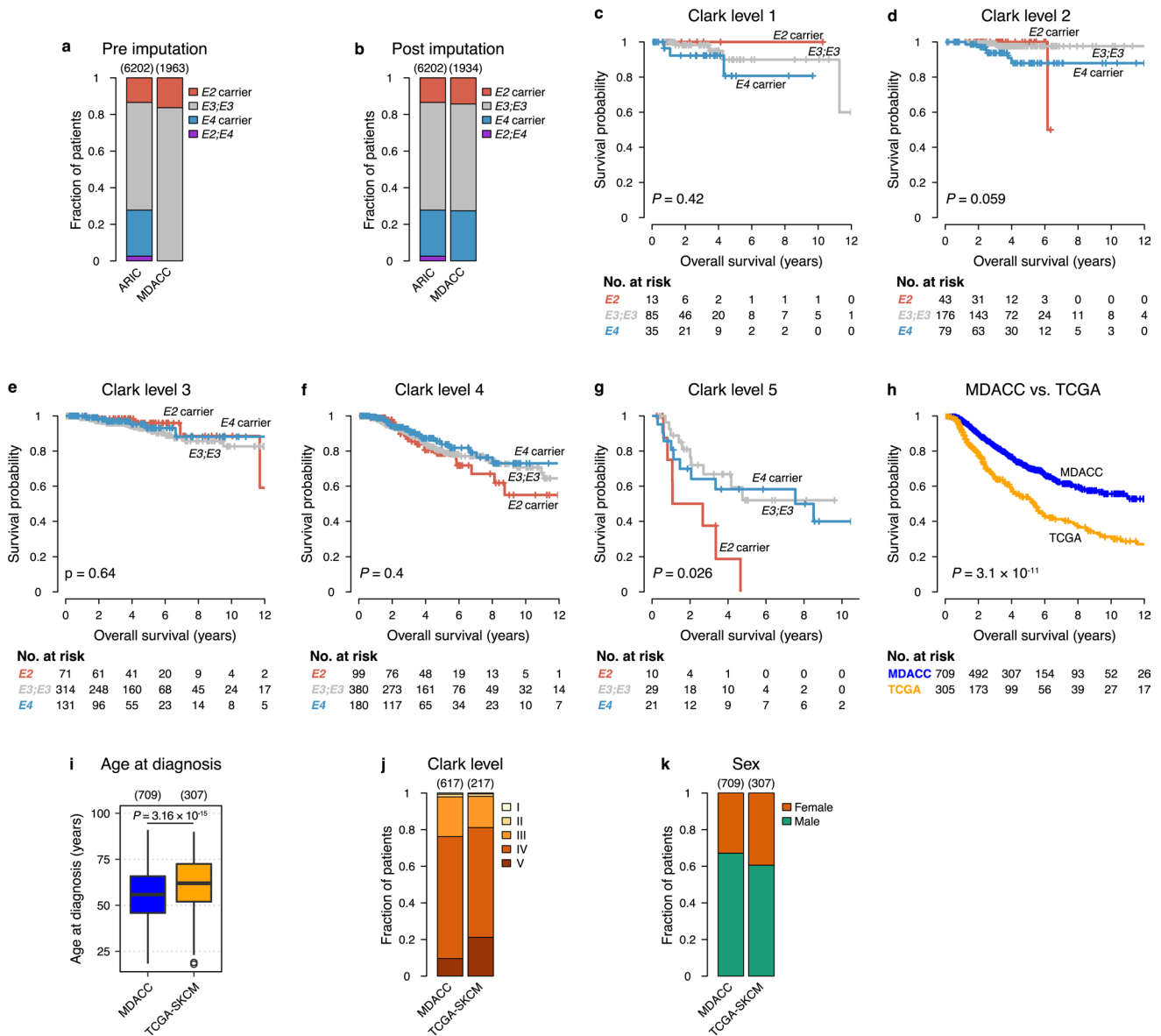
Extended Data Fig. 6 | Distribution of APOE genotype in the TCGA-SKCM study. a-b, Proportion of APOE2 and APOE4 carrier status (**a**) and bi-allelic genotype (**b**) in the Atherosclerosis Risk in Communities study (ARIC) and in patients with stage II/III melanoma in the TCGA-SKCM study ($P=0.0017$ and 0.0066 , respectively; χ^2 test).



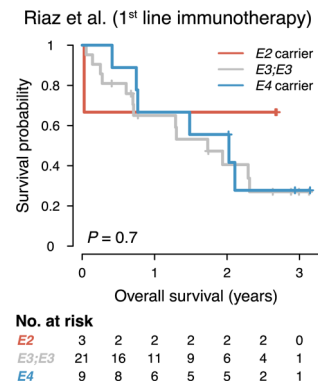
Extended Data Fig. 7 | Clinical characteristics of stage II/III patients in the TCGA-SKCM study. **a**, Sex proportions were not significantly different between *APOE* carrier groups ($P=0.46$, χ^2 test). **b**, Age at diagnosis was not significantly different between *APOE* carrier groups ($P=0.45$, Kruskal-Wallis rank sum test). **c**, Tumor stage at diagnosis was not significantly different between *APOE* carrier groups ($P=0.4$, χ^2 test). **d**, Melanoma Clark level at diagnosis was not significantly different between *APOE* carrier groups ($P=0.95$, χ^2 test). **e**, Breslow depth was not significantly different between *APOE* carrier groups at diagnosis ($P=0.24$, Kruskal-Wallis rank sum test). **f**, *APOE* carrier status was not significantly associated with common tumor mutations ($P=0.93$, χ^2 test). **g**, *APOE* carrier status was not significantly associated with transcriptomic cluster ($P=0.55$, χ^2 test). **h**, Univariate analysis of the impact of clinical and molecular characteristics on survival of stage II/III melanoma patients (P values according to univariate Cox proportional hazards model). **i**, Multivariable analysis of the impact of clinical and molecular characteristics with significant impact in univariate analysis on survival of stage II/III melanoma patients (P values according to multivariable Cox proportional hazards model). For (**h-i**), the number of patients with available information for a given characteristic is indicated in column “ n ”, and plots represent hazard ratios with 95% confidence intervals. Hinges of boxplots represent the first and third quartiles, whiskers extend to the smallest and largest value within $1.5 \times$ interquartile ranges of the hinges, and points represent outliers.



Extended Data Fig. 8 | APOE genotype in normal tissue versus tumor samples of stage II/III patients in the TCGA-SKCM study. a, Proportion of APOE2 and APOE4 carrier status in normal tissue and tumor samples of patients with stage II/III melanoma in the TCGA-SKCM study ($P = 0.8899$; χ^2 test). **b**, Chord diagram of APOE carrier status as identified in paired normal and tumor tissue samples of stage II/III melanoma patients in the TCGA-SKCM study.



Extended Data Fig. 9 | Characteristics of the MDACC GWAS study and comparison to TCGA-SKCM. **a–b**, Distribution of *APOE* carrier status in the Atherosclerosis Risk in Communities study (ARIC) and the MDACC melanoma study before (**a**) and after (**b**) imputation of *APOE* genotype ($P < 2.2 \times 10^{-16}$ and $P = 1.82 \times 10^{-11}$, respectively; χ^2 test). **c–g**, Survival of melanoma patients in the MDACC study stratified by local melanoma stage and *APOE* genotype (two-sided log-rank tests). **h**, Survival of stage II/III melanoma patients in the MDACC and TCGA-SKCM studies (two-sided log-rank test). **i–k**, Distribution of age (**i**), melanoma Clark level (**j**), and sex (**k**) in stage II/III patients of the MDACC and TCGA-SKCM melanoma studies (respective significance tests: $P = 6.42 \times 10^{-9}$, Kruskal-Wallis rank sum test; $P = 0.0005$, χ^2 test; $P = 0.052$, χ^2 test). Hinges of boxplots represent the first and third quartiles, whiskers extend to the smallest and largest value within $1.5 \times$ interquartile ranges of the hinges, and points represent outliers.



Extended Data Fig. 10 | Association of APOE genotype with outcome in upfront anti-PD1 immunotherapy-treated melanoma patients. Survival of melanoma patients treated with anti-PD1 therapy with no prior checkpoint therapy from the Riaz et al. study (P value according to two-sided log-rank test).

Reporting Summary

Nature Research wishes to improve the reproducibility of the work that we publish. This form provides structure for consistency and transparency in reporting. For further information on Nature Research policies, see [Authors & Referees](#) and the [Editorial Policy Checklist](#).

Statistics

For all statistical analyses, confirm that the following items are present in the figure legend, table legend, main text, or Methods section.

n/a Confirmed

- The exact sample size (n) for each experimental group/condition, given as a discrete number and unit of measurement
- A statement on whether measurements were taken from distinct samples or whether the same sample was measured repeatedly
- The statistical test(s) used AND whether they are one- or two-sided
Only common tests should be described solely by name; describe more complex techniques in the Methods section.
- A description of all covariates tested
- A description of any assumptions or corrections, such as tests of normality and adjustment for multiple comparisons
- A full description of the statistical parameters including central tendency (e.g. means) or other basic estimates (e.g. regression coefficient) AND variation (e.g. standard deviation) or associated estimates of uncertainty (e.g. confidence intervals)
- For null hypothesis testing, the test statistic (e.g. F , t , r) with confidence intervals, effect sizes, degrees of freedom and P value noted
Give P values as exact values whenever suitable.
- For Bayesian analysis, information on the choice of priors and Markov chain Monte Carlo settings
- For hierarchical and complex designs, identification of the appropriate level for tests and full reporting of outcomes
- Estimates of effect sizes (e.g. Cohen's d , Pearson's r), indicating how they were calculated

Our web collection on [statistics for biologists](#) contains articles on many of the points above.

Software and code

Policy information about [availability of computer code](#)

Data collection

AlphaView v3.4 (Protein Simple); Living Image v4.5 (Perkin Elmer); FACSDiva v8 (BD Biosciences)

Data analysis

Analysis of previously published whole-exome sequencing data (TCGA-SKCM, Roh et al. and Riaz et al. studies) was performed using RStudio v1.1.3, R v3.5, samtools/bcftools 1.8, and the R packages 'TCGAbiolinks'/'survival'/'survminer' as outlined in the methods section. Analysis of the MDACC GWAS study was performed using Plink v1.9, GenotypeHarmonizer v1.4.2, Shapelt v2, and Impute2 as outlined in the methods section. Single cell RNA-sequencing was analyzed using Cell ranger v3.0.1 and Seurat v3.0.2. Gene set enrichment analysis was performed using the R package clusterProfiler v3.12. Flow cytometry data were analyzed with Flowjo v9.3. Immunofluorescent images for Endomucin and CD8+ stainings were analyzed using CellProfiler v3.1.8. All other graphs were generated using Graphpad Prism v8. Microsoft Excel v16 was used for data processing and t-test calculation.

For manuscripts utilizing custom algorithms or software that are central to the research but not yet described in published literature, software must be made available to editors/reviewers. We strongly encourage code deposition in a community repository (e.g. GitHub). See the Nature Research [guidelines for submitting code & software](#) for further information.

Data

Policy information about [availability of data](#)

All manuscripts must include a [data availability statement](#). This statement should provide the following information, where applicable:

- Accession codes, unique identifiers, or web links for publicly available datasets
- A list of figures that have associated raw data
- A description of any restrictions on data availability

All data analyzed from published studies are publicly available under the following accession numbers: TCGA-SKCM, dbGaP accession phs000178.v10.p8; MDACC GWAS study, phs000187.v1.p1; Roh et al. anti-PD1 treatment study, dbGaP BioProject ID PRJNA369259; Riaz et al. anti-PD1 treatment study, dbGaP BioProject ID PRJNA359359. Single-cell RNA-sequencing data has been deposited at the Gene Expression Omnibus (GEO) under accession number GSE146613. All other data are available from the corresponding author upon request.

Field-specific reporting

Please select the one below that is the best fit for your research. If you are not sure, read the appropriate sections before making your selection.

Life sciences Behavioural & social sciences Ecological, evolutionary & environmental sciences

For a reference copy of the document with all sections, see [nature.com/documents/nr-reporting-summary-flat.pdf](https://www.nature.com/documents/nr-reporting-summary-flat.pdf)

Life sciences study design

All studies must disclose on these points even when the disclosure is negative.

Sample size	The number of samples for each group was empirically chosen based on knowledge on intragroup variation and expected effect size. Sample sizes for in-vitro experiments were chosen based on prior knowledge on intragroup variation (e.g., invasion and endothelial recruitment assays). No statistical methods were used to predetermine sample sizes.
Data exclusions	No data were excluded.
Replication	All in-vitro experiments were performed at least three times with similar results, and in-vivo experiments were performed at least twice with similar results.
Randomization	Samples were allocated randomly if possible. For experiments with genetically modified mice, allocation was performed according to genotype and mice were sex- and age-matched.
Blinding	Investigators were blinded for data collection for all in-vitro assays. No blinding was performed for in-vivo experiments due to cage labeling requirements.

Reporting for specific materials, systems and methods

We require information from authors about some types of materials, experimental systems and methods used in many studies. Here, indicate whether each material, system or method listed is relevant to your study. If you are not sure if a list item applies to your research, read the appropriate section before selecting a response.

Materials & experimental systems

n/a	Involved in the study
<input type="checkbox"/>	<input checked="" type="checkbox"/> Antibodies
<input type="checkbox"/>	<input checked="" type="checkbox"/> Eukaryotic cell lines
<input checked="" type="checkbox"/>	<input type="checkbox"/> Palaeontology
<input type="checkbox"/>	<input checked="" type="checkbox"/> Animals and other organisms
<input checked="" type="checkbox"/>	<input type="checkbox"/> Human research participants
<input checked="" type="checkbox"/>	<input type="checkbox"/> Clinical data

Methods

n/a	Involved in the study
<input checked="" type="checkbox"/>	<input type="checkbox"/> ChIP-seq
<input type="checkbox"/>	<input checked="" type="checkbox"/> Flow cytometry
<input checked="" type="checkbox"/>	<input type="checkbox"/> MRI-based neuroimaging

Antibodies

Antibodies used	CD45-BV785 (clone: 30-F11, supplier: BioLegend, cat#: 103149, lot#: B263597, dilution: 1:3,000), B220-BUV395 (RA3-6B2, BD Biosciences, 563793, 7177756, 1:400), CD11b-BV605 (M1/70, BioLegend, 101257, B256673, 1:6,000), CD11b-FITC (M1/70, BioLegend, 101206, B192968, 1:4,000), Ly6G-PerCP/Cy5.5 (1A8, Biolegend, 127616, B196548, 1:500), Ly6C-BV711 (HK1.4, BioLegend, 128037, B264621, 1:12,000), I-A/I-E-BV421 (M5/114.15.2, BioLegend, 107632, B234681, 1:9,000), F4/80-FITC (BM8, BioLegend, 123108, B222019, 1:500), CD24-PE (M1/69, BioLegend, 101808, B180221, 1:5,000), CD103-APC (2E7, BioLegend, 121414, B236942, 1:500), CD19-FITC (1D3/CD19, BioLegend, 152404, B233717, 1:1,500), TCR β -PerCP/Cy5.5 (H57-597, BioLegend, 109228, B227995, 1:200), CD49b-APC (HMa2, BioLegend, 103516, B230857, 1:300), CD4-BV605 (GK1.5, BioLegend, 100451, B246547, 1:200), CD8 α -AF700 (53-6.7, BioLegend, 100730, B205738, 1:1,000), Granzyme B-PE (QA16A02, BioLegend, 372208, B265797, 1:200), IFN γ -PE/Cy7 (XMG1.2, eBioscience, 25-7311-82, 4273965, 1:500), anti-Endomucin (V.7C7, Santa Cruz, sc-65495, F2618, 1:200), anti-CD8 (polyclonal, Synaptic Systems, 361003, 1:200).
Validation	Validation data of the antibodies listed above was performed by the manufacturers and is available at each manufacturer's website by searching under the provided antibody catalog numbers.

Eukaryotic cell lines

Policy information about [cell lines](#)

Cell line source(s)	B16F10, YUMM3.3, HUVEC, and Mewo cells were obtained from ATCC. YUMM1.7 and YUMMER1.7 cells were a gift from M. Bosenberg (Yale University).
---------------------	--

Authentication	BRAF mutation present in the YUMM1.7 cell was validated by genotyping PCR. No other independent authentication was performed.
Mycoplasma contamination	Mycoplasma contamination in the cell lines was ruled out by regular PCR-based mycoplasma testing.
Commonly misidentified lines (See ICLAC register)	None.

Animals and other organisms

Policy information about [studies involving animals](#); [ARRIVE guidelines](#) recommended for reporting animal research

Laboratory animals	Human APOE-knock-in mice were obtained from Taconic Biosciences. C57Bl6j mice were obtained from Jackson laboratories. Mice for primary tumor growth and experimental metastasis assays were used at 7-10 weeks of age and were age- and sex-matched.
Wild animals	No wild animals were used in this study.
Field-collected samples	No field-collected samples were used in this study.
Ethics oversight	All animals experiments were conducted in accordance with a protocol approved by the Institutional Animal Care and Use Committee at The Rockefeller University.

Note that full information on the approval of the study protocol must also be provided in the manuscript.

Flow Cytometry

Plots

Confirm that:

- The axis labels state the marker and fluorochrome used (e.g. CD4-FITC).
- The axis scales are clearly visible. Include numbers along axes only for bottom left plot of group (a 'group' is an analysis of identical markers).
- All plots are contour plots with outliers or pseudocolor plots.
- A numerical value for number of cells or percentage (with statistics) is provided.

Methodology

Sample preparation	Tumor-infiltrating leukocytes were isolated using enzymatic digestion and Percoll gradient centrifugation as outlined in the methods section.
Instrument	BD LSR Fortessa
Software	BD DIVA software v8 was used for data collection and Flowjo software v9.3 was used for data analysis.
Cell population abundance	Cell population abundances in the post-sort fraction were not assessed.
Gating strategy	A gating strategy was followed as outlined in Supplementary Data Fig 2. In brief, an initial gate based on basal scatter characteristics served to exclude debris followed by singlet gates based on FSC-H and SSC-H. Compensation was calculated using single color controls using Ultracomp compensation beads (ThermoFisher) for antibodies and amine-reactive beads for Zombie (ThermoFisher).

- Tick this box to confirm that a figure exemplifying the gating strategy is provided in the Supplementary Information.